5

Fault Tolerant Flight Control, a Physical Model Approach

Thomas Lombaerts, Ping Chu,
Jan Albert (Bob) Mulder and Olaf Stroosma
Delft University of Technology
the Netherlands

1. Introduction

Safety is of paramount importance in all transportation systems, but especially in civil aviation. Therefore, in civil aviation, a lot of developments focus on the improvement of safety levels and reducing the risks that critical failures occur. When one analyses recent aircraft accident statistics (*Civil Aviation Safety Data 1993-2007* (2008); Smaili et al. (2006)), there are two major categories of accidents which can be attributed to a single primary cause, as illustrated in figure 1. The largest category is "collision with ground" (controlled flight into terrain, CFIT) where a fully functional aircraft hits terrain due to the loss of situational awareness by the pilot, which counts for as much as 26% of the accidents. This percentage is decreasing over the years thanks to the continuously evolving amount and manner of cockpit display information. The second major category is "loss of control in flight", which can be attributed to mistakes made by the pilot or a technical malfunctioning. This category counts for 16% of all aircraft accident cases and is not decreasing.

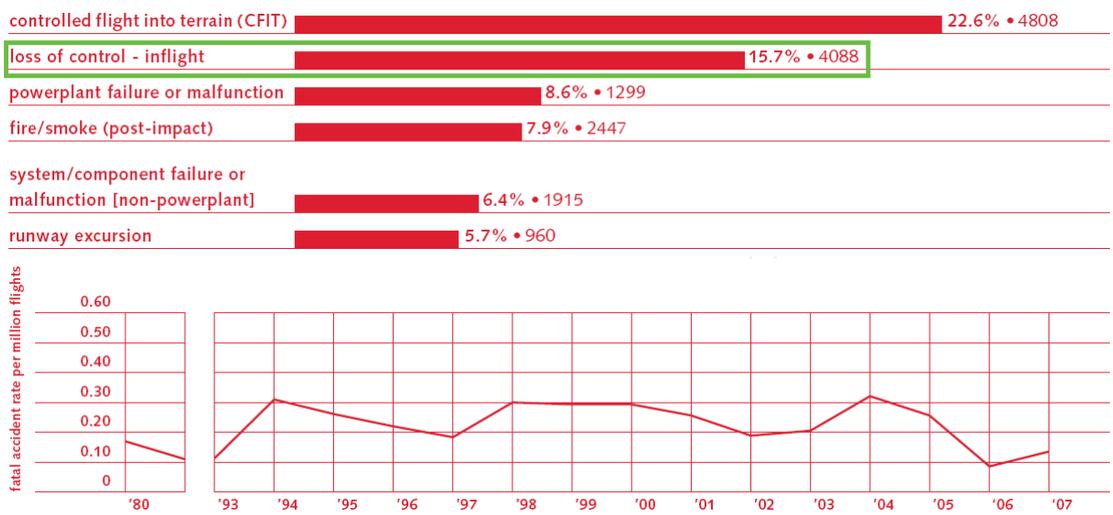

Fig. 1. Accident statistics, source: *Civil Aviation Safety Data 1993-2007* (2008)

Analysing a major part of the accidents in the latter category has led to a common conclusion: from a flight dynamics point of view, with the technology and computing power available at this moment, it might have been possible to recover the aircraft in many accident situations in this category, on the condition that non-conventional control strategies would have been available. These non-conventional control strategies involve the so-called concept of active fault tolerant flight control (FTFC), where the control system is capable to detect the change in the aircraft behaviour and to adapt itself so that it can handle the perturbed aircraft dynamics. Earlier research projects in FTFC involve the Self-Repairing Flight Control System (SRFCS) program (Corvin et al. (1991)), the MD-11 Propulsion Controlled Aircraft (PCA) (KrishnaKumar & Gundy-Burlet (n.d.)), the Self-Designing Controller for the F-16 VISTA (Ward & Barron (1995)), Reconfigurable Systems for Tailless Fighter Aircraft in the X-36 RESTORE program (Brinker & Wise (1999); Calise et al. (2001)), the NASA Intelligent Flight Control System (IFCS) F-15 program (*Intelligent Flight Control: Advanced Concept Program* (1999)) and Damage Tolerant Flight Control Systems for Unmanned Aircraft by Athena/Honeywell (Gavrilets (2008)). There are many alternative control approaches to achieve FTFC. In all these control approaches, there remain some problems and limitations, varying from the limitation to a restricted number of failure cases to the limitation of the type and extent of damage which can be compensated for due to fixed model structures for identification. Another frequently encountered issue are convergence problems. Besides, black box structures like for neural networks reduce the transparency of the approach. Moreover, for many approaches it is not clear what will happen when the reference model behaviour is not achievable in post-failure conditions.

The research approach as elaborated in this chapter uses a physical modular approach, where focus is placed on the use of mathematical representations based on flight dynamics. All quantities and variables which appear in the model have a physical meaning and thus are interpretable in this approach, and one avoids so-called black and grey box models where the content has no clear physical meaning. Besides the fact that this is a more transparent approach, allowing the designers and engineers to interpret data in each step, it is assumed that these physical models will facilitate certification for eventual future real life applications, since monitoring of data is more meaningful.

Adaptive nonlinear dynamic inversion has been selected as the preferred adaptive control method in this modular or indirect approach. The advantages of dynamic inversion are the absence of any need for gain scheduling, and an effective input-output decoupling of all control channels. Adaptation of the controller is achieved by providing up-to-date aerodynamic model information which is collected in a separate identification module.

The structure of this chapter is as follows. Section 2 provides information on the high fidelity RECOVER simulation model which has been used in this research project. A global overview of the fault tolerant control architecture is given in section 3, and further explanations of some of the individual modules are added in sections 4 and 5. Simulation results are discussed in section 4.2 for the aerodynamic model identification, section 5.3 for the autopilot and in section 5.5 for the manual control approach. Finally, section 6 presents some conclusions and recommendations for future research.

2. The RECOVER benchmark simulation model

The presented work is part of a research project by the Group for Aeronautical Research and Technology in Europe (GARTEUR). This group has established flight mechanics action group FM-AG(16) with the specific goal to investigate the possibilities of fault tolerant control in aeronautics and to compare the results of different reconfiguring control strategies applied to a reference benchmark flight trajectory. That benchmark scenario is inspired by the so-called

Bijlmermeer disaster of EL AL flight 1862, where a Boeing 747-200 Cargo aircraft of Israel's national airline EL AL lost two engines immediately after take-off from Amsterdam airport Schiphol in the Netherlands and crashed into an apartment building in the neighbourhood while trying to return to the airport. A detailed simulation model of this damaged aircraft is available from the Dutch Aerospace Laboratory NLR. This RECOVER (REconfigurable COntrol for Vehicle Emergency Relief) benchmark model is discussed in detail in ref. Smaili et al. (2008; 2006) and has been used (also in earlier versions) by a number of investigators and organizations (Maciejowski & Jones (2003); Marcos & Balas (2003); Szaszi et al. (2002)). More information about the reference benchmark scenario can be found in ref. Lombaerts et al. (2005; 2006). Other control strategies and results applied to the same benchmark model as part of the framework of FM-AG(16) can be found in ref. Alwi (2008); Cieslak et al. (2008); Hallouzi & Verhaegen (2008); Joosten et al. (2007; 2008). Related FDI work can be found in ref. Varga (2007); Varga & Hecker (2004).
The simulation benchmark for evaluating fault tolerant flight controllers as discussed in ref. Smaili et al. (2006) contains six benchmark fault scenarios, enumerated in fig. 2(a). These failure cases have varying criticality. Fig. 2(b) shows the failure modes and structural damage configuration of the Flight 1862 accident aircraft, which is the most important fault scenario in the simulation benchmark.

Failure mode	Reconfiguration	Criticality
No failure	N/A	None
Stuck or erroneous elevator	Stabiliser Ailerons (symmetric) Differential thrust	Major
Stuck or erroneous aileron	Ailerons (other) Spoilers	Major
Elevator/stabiliser runaway	Elevator Ailerons Flaps Thrust Use of static stability	Catastrophic
Stuck, erroneous or rudder runaway	Remaining surfaces Asymmetric thrust	Catastrophic
Loss of vertical tail surface	Differential thrust Differential Speedbrakes	Catastrophic
Engine separation & structural damage	Remaining surfaces Remaining engines Remaining sensors	Catastrophic

(a) GARTEUR FM-AG(16) RECOVER benchmark fault scenarios, source: Smaili et al. (2008)

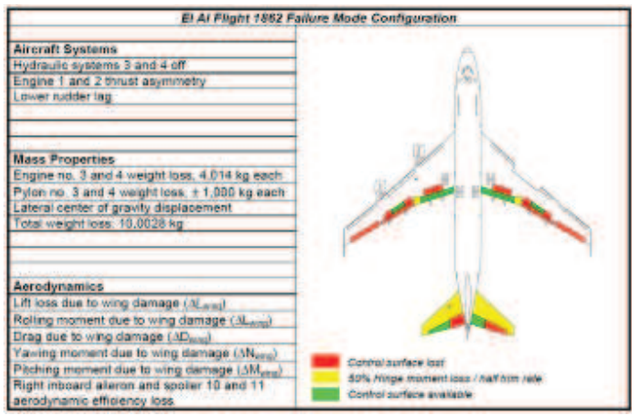

(b) Failure modes and structural damage configuration of the Flight 1862 accident aircraft, suffering right wing engine separation, partial loss of hydraulics and change in aerodynamics, source: Smaili et al. (2008)

Fig. 2. GARTEUR FM-AG(16) RECOVER benchmark fault scenarios and configuration

The rudder runaway, the vertical tail separation and the EL AL engine separation have been used as scenarios for this chapter. In the case of a rudder runaway (also called hardover), the rudder moves quickly to an extreme position. More precisely, the rudder deflects to the left, inducing a yawing tendency of the aircraft to the left. The rudder deflection limit in this scenario depends on the flight speed, since aerodynamic blowdown is taken into account in the RECOVER simulation model. As a result the maximum rudder deflection is slightly below 15° for an airspeed around 270 knots, and even close to 25° (the physical maximum deflection limit imposed by the rudder hardware structure) for an airspeed of 165 knots. The vertical tail separation leads to the loss of all rudder control surfaces as well as the loss of all damping in the roll and yaw axes. Mind that loss of hydraulics is not considered in this situation. The El Al engine separation scenario is an accurate simulation of flight 1862, validated by black box data of the accident, where the loss of hydraulics is taken into account.

3. Global overview of the physical modular approach

Globally, the overall architecture of this modular approach consists of three major assemblies, namely the controlled system, the Fault Detection and Identification (FDI) assembly and the Fault Tolerant Flight Control (FTFC) assembly, as shown in fig. 3. The controlled system comprises the aircraft model and the actuator hardware. Possible failures in this controlled system are structural failures and actuator hardware failures in the latter. Sensor failures have not been considered in this research, since it has been assumed that effects of these failures can be minor thanks to sensor redundancy and sensor loss detection. However, the latter mechanism is recommended for future research.

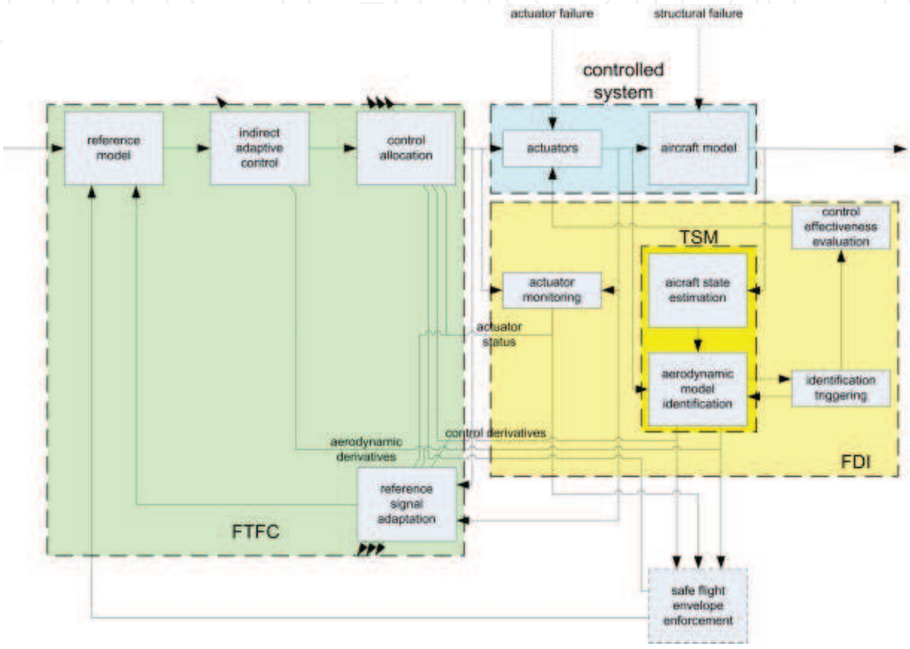

Fig. 3. Overview of the modular physical approach for fault tolerant flight control

The Fault Detection and Identification (FDI) architecture consists of several components. The core of this assembly is the two step method (TSM) module, described in section 4.1. This module consists of a separate aircraft state estimation step followed by an aerodynamic model identification step, where the latter is a joint structure selection and parameter estimation (SSPE) procedure. The state estimation step is a nonlinear problem solved by an Iterated Extended Kalman Filter. The preferred SSPE algorithm is Adaptive Recursive Orthogonal Least Squares. In case a structural failure occurs (in the aircraft structure or in one of the control surfaces), re-identification is triggered when the average square innovation exceeds a predefined threshold. For successful identification of the control derivatives of every individual control surface, control effectiveness evaluation is needed after failure. This can be done by inserting multivariate orthogonal input signals in the actuators. Although this must be done carefully such that the damaged aircraft cannot be destabilized, it is necessary in order to obtain sufficient control surface efficiency information for the control allocation module, to be discussed later. A valid approach might be to introduce these evaluation signals only when strictly needed, i.e. when successful reconfiguration is not possible due to a lack of information about this control efficiency. The two step method is ideally suited to deal with structural failures, but for the detection of actuator failures a separate actuator monitoring algorithm is needed, such as an Actuator Health Monitoring System (AHMS).

Four other functions can be grouped to form the Fault Tolerant Flight Control (FTFC) assembly. The core for this group are indirect adaptive control and control allocation. Indirect adaptive control can be achieved by adaptive nonlinear dynamic inversion (ANDI) described in section 5.1. In this setup, the control structure consists of three inversion loops, as elaborated in section 5.2. This control structure relies on the principle of time scale separation. The advantages of ANDI are that it removes the need for gain scheduling over different operating conditions and it effectively decouples input-output relationships. Moreover, the NDI control algorithm automatically involves some form of control allocation, due to the structure of the control law. This structuring allows a clear separation how different failure types are dealt with. Structural failures independent of the control surfaces are detected by the TSM and this damage information is supplied to the ANDI algorithm by means of the aerodynamic derivatives. On the other hand control surface related failures, aerodynamics or actuator related, are identified by the TSM or the actuator monitoring algorithm respectively. This information is sent to the adaptive control allocation block. The preferred control allocation approach is found to be the control distributor concept (CDC), (Oppenheimer & Doman (2006)), combined with the weighted pseudo inverse (WPI). This method assumes the presence of a large amount of similar control surfaces. This assumption holds for the type of aircraft considered in this research project, such as the Boeing 747. This approach fits in the modular setup of the global procedure, where the CDC principle takes into account aerodynamic changes and the WPI provides the adaptivity with reference to actuator failures. Furthermore, a reference model defines the reference signal that the closed loop configuration has to track. However, this reference model needs to be adaptive such that its signals are limited based upon the achievable performance of the damaged closed loop configuration. This reference signal adaptation can be achieved by Pseudo Control Hedging. This modulation is based upon the difference between the demanded input signal and the achieved input signal by the actuators. This reference signal adaptation is primarily driven by saturation effects. Besides, this hedging operation takes into account the updated model information from the FDI assembly. In this way, one makes sure that no unreachable reference signals are given to the closed loop configuration. This PCH operation can be considered as a first degree of safe flight envelope enforcement, based upon input saturation effects and updated model information. Experiments have shown that especially the throttle channel is prone to saturation effects.

During this research, it has been found that safe flight envelope enforcement is a crucial aspect in this control setup, and it is part of recommended future research. This protection algorithm, based upon the achievable performance which can be estimated based upon actuator status, aerodynamic derivatives and control derivatives, should contribute on two levels. On one hand, it has to assist the PCH algorithm by limiting the reference model output appropriately. Moreover, the output of the control allocation block, and thus the input to the actuators, should be limited based upon this reachable flight envelope information. A tabular overview of the preferred method for every component in the global overview of the fault tolerant flight control setup can be found in table 1.

In the following sections, further explanations will be given about some of the individual modules.

4. Fault detection and identification

4.1 Two step method

The identification method considered in this study is the so-called two step method (Chu (2007); Chu et al. (1994); Laban (1994); Mulder (1986); Mulder et al. (1999)). There are many other identification algorithms mentioned in the literature like maximum likelihood

component	preferred method
aircraft state estimation	Iterated Extended Kalman Filter
aerodynamic model identification	Adaptive Recursive Orthogonal Least Squares
identification triggering	average square innovation & threshold
control effectiveness evaluation	multivariate orthogonal input functions
control allocation	Control Distributor Concept & Weighted Pseudo Inverse
indirect adaptive control	triple layer Adaptive Nonlinear Dynamic Inversion
actuator monitoring	Actuator Health Monitoring System
reference signal adaptation	Pseudo Control Hedging

Table 1. Preferred methods for FTFC modules

identification (MLI) and other one step identification routines, but not all of them are applicable on line. One of the few procedures which can be implemented in real time is the so-called filtering method developed at German Aerospace Centre DLR, see ref. Jategaonkar (2006). This is a joint state and parameter estimation algorithm, but very complex. Another algorithm can be found in ref. Morelli (2000), which is frequency based. The advantage of the two step method is that it is easier to implement on-line. The aim is to update an a priori aerodynamic model (obtained by means of windtunnel tests and CFD calculations) by means of on-line flight data. The first step is called the Aircraft State Estimation phase, where the second one is the Aerodynamic Model Identification step. In the Aircraft State Estimation procedure, an Iterated Extended Kalman Filter is used to determine the aircraft states, by making use of the redundant but perturbed information from all sensors (air data, inertial, magnetic and GPS measurements). By means of this state information, it is possible to construct the combined aerodynamic and thrust forces and moments acting on the aircraft. Mass and inertia are considered as known constants in these calculations. In the absence of a structural failure, real time mass and inertia can be calculated by integrating fuel flow and subtracting it from the total take off values. Future research is aimed at taking into account changing masses and inertia in the presence of structural failures. Finally the aerodynamic derivatives can be deduced in the second step by means of structure selection and parameter estimation.

This second step involves the aerodynamic properties of the aircraft. Thanks to the separation of the kinematics, these aerodynamics become linear in the parameters. Model structure determination is the first concern, and a regression method can be applied in order to estimate the so-called aerodynamic model parameters. Simultaneous recursive structure selection and parameter estimation is performed in this phase, by means of so-called Adaptive Recursive Orthogonal Least Squares (AROLS), (Lombaerts et al. (2010c)). This method determines the model structure by means of an orthogonal **QR**-decomposition, which is extended recursively to make the method suitable for online applications. Special monitoring criteria verify continuously when the structure needs to be extended. For a detailed discussion of these criteria see ref. Lombaerts et al. (2010c).

The model structure selection procedure considers a set of candidate regressors based upon a Taylor series expansion with respect to the aircraft states and control inputs (control surface deflections and engine settings) relevant for the aerodynamic forces and moments. The candidate regressors are shown in table 2.

dependent variable	candidate regressors
X; Z; M	$1, \alpha, \alpha^2$ (X only), $\frac{q\bar{c}}{V}, \delta_{e_i}, i_h, \delta_{sp_i}, \delta_{f_i}, T_i$ $\{\beta, \frac{pb}{2V}, \frac{rb}{2V}, \alpha^m, \alpha\frac{q\bar{c}}{V}, \alpha\delta_e, \alpha\beta, \alpha\beta^2, \alpha^2\beta, \alpha\beta^3, \alpha^2\beta^3 \quad m = 3, \ldots, 8\}$ $\{\alpha\frac{pb}{2V}, \alpha\frac{rb}{2V}, \alpha^2\frac{pb}{2V}, \alpha^2, \frac{rb}{2V}, \beta^n \quad n = 2, \ldots, 5\}$
Y; L; N	$1, \beta, \frac{pb}{2V}, \frac{rb}{2V}, \delta_{a_i}, \delta_{r_i}, \delta_{sp_i}, \{\alpha, \frac{q\bar{c}}{V}, T_i\}$ $\{\alpha^m, \alpha\frac{q\bar{c}}{V}, \alpha\delta_e, \alpha\beta, \alpha\beta^2, \alpha^2\beta, \alpha\beta^3, \alpha^2\beta^3 \quad m = 2, \ldots, 8\}$ $\{\alpha\frac{pb}{2V}, \alpha\frac{rb}{2V}, \alpha^2\frac{pb}{2V}, \alpha^2, \frac{rb}{2V}, \beta^n \quad n = 2, \ldots, 5\}$

Table 2. States and control inputs which influence forces and moments

	β	p	r	δ_a	δ_r	
Y	$C_{Y_\beta} < 0$	$C_{Y_p} \approx 0$	$C_{Y_r} > 0$	$C_{Y_{\delta_a}} \approx 0$	$C_{Y_{\delta_r}} > 0$	nominal
	$C_{Y_\beta} \ll 0$	$C_{Y_p} \approx 0$	$C_{Y_r} > 0$	$C_{Y_{\delta_a}} \approx 0$	$C_{Y_{\delta_r}} > 0$	engine separation
	$C_{Y_\beta} \leq 0$	$C_{Y_p} \approx 0$	$C_{Y_r} \geq 0$	$C_{Y_{\delta_a}} \approx 0$	$C_{Y_{\delta_r}} = 0$	tail loss
L	$C_{l_\beta} < 0$	$C_{l_p} < 0$	$C_{l_r} > 0$	$C_{l_{\delta_a}} < 0$	$C_{l_{\delta_r}} > 0$	nominal
	$C_{l_\beta} < 0$	$C_{l_p} \leq 0$	$C_{l_r} \gg 0$	$C_{l_{\delta_a}} < 0$	$C_{l_{\delta_r}} > 0$	engine separation
	$C_{l_\beta} \leq 0$	$C_{l_p} < 0$	$C_{l_r} > 0$	$C_{l_{\delta_a}} < 0$	$C_{l_{\delta_r}} = 0$	tail loss
N	$C_{n_\beta} > 0$	$C_{n_p} < 0$	$C_{n_r} < 0$	$C_{n_{\delta_a}} > 0$	$C_{n_{\delta_r}} < 0$	nominal
	$C_{n_\beta} \gg 0$	$C_{n_p} < 0$	$C_{n_r} < 0$	$C_{n_{\delta_a}} > 0$	$C_{n_{\delta_r}} < 0$	engine separation
	$C_{n_\beta} \leq 0$	$C_{n_p} < 0$	$C_{n_r} \leq 0$	$C_{n_{\delta_a}} > 0$	$C_{n_{\delta_r}} = 0$	tail loss

Table 3. Predicted lateral aerodynamic derivative changes for asymmetric failure scenarios studied

In table 2, $\{\ldots\}$ indicate regressor candidates for AROLS related to aerodynamic cross coupling effects in case of aircraft asymmetries as well as higher order aerodynamic effects, for example due to structural failures. The identified parameters contain valuable information about the physical state of the aircraft. For example, the parameters C_{m_α} and C_{n_β} represent measures for static stability. In fact, C_{n_β} is also known as Weathercock stability. The derivatives $C_{m_{\delta_e}}$, $C_{l_{\delta_a}}$ and $C_{n_{\delta_r}}$ represent "elevator-", "aileron-" and "rudder-effectiveness" respectively.
A structural failure will result in changing aerodynamic derivatives. Based upon flight dynamics theory (Mulder et al. (January 2006)), it is possible to predict the changes in the aerodynamic derivatives in the engine separation and tail loss scenarios, as illustrated in table 3. Each parameter is an aerodynamic derivative, e.g. C_{Y_β} represents the change in lateral force Y caused by a change in sideslip angle β. In the engine separation scenario for example, wing sweep combined with the loss of the leading edge results in a larger negative Y-force caused by a positive sideslip angle β.
Various validation tests by means of a posteriori batch process identification, least squares residual analysis and reconstruction of velocity and angular rate components have shown that this method works well and can in fact be used for identification purposes of damaged aircraft. Identification of component as well as structural failures is possible in this setting, see ref Lombaerts et al. (2007) for a more elaborate discussion of validation methods and results.

4.2 Applications

Two application examples are considered here. First, a static directional stability analysis is performed for the tail loss scenario. Thereafter, the model structure of the dimensionless

aerodynamic force coefficient C_Z is elaborated and its parameter values are estimated at the same moment in the engine separation scenario.

4.2.1 Tail loss

A natural consequence of the tail loss scenario is the huge reduction in directional static stability. This can be seen in the behaviour of the aerodynamic derivative C_{n_β}, as shown in fig. 4. A positive value for C_{n_β} indicates static directional stability. From fig. 4, it is clear that, while the nominal aircraft is stable, the damaged aircraft is observed to be directionally statically unstable.

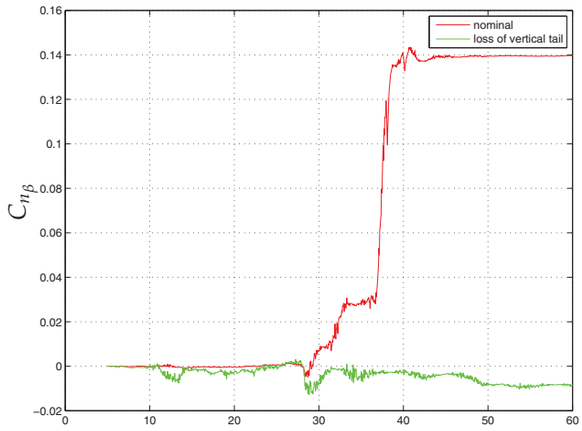

Fig. 4. Comparison of Weathercock stability derivative for undamaged and damaged aircraft with loss of vertical tail

4.2.2 Engine separation

In this example, the dimensionless aerodynamic force coefficient C_Z is considered in the engine separation scenario. Applying the AROLS routine to this stretch of simulation data leads to the results as shown in fig. 5. Fig. 5(a) shows the results prior to failure, while fig. 5(b) focuses on the post-failure situation. As can be seen in this figure, the fit is accurate in both cases. The optimal residual, which is updated over the entire time history at every time step, is minimal. The real residual, which is not updated a posteriori, gives an indication of the reduction in the residual over the time interval. Fig. 5(a) reveals the initial large residual due to initialization. Fig. 5(b) shows the initial large residual caused by the failure. This is minimized in very short term, but starts increasing thereafter due to slow dynamics which become dominant. Between 55s and 60s, the residual is again minimized, thanks to the incorporation of these slow dynamics in the aerodynamic model.

The parameter estimation results, together with their standard deviations, can be found in table 4. These results highlight the difference between the situations before and after failure. Because there is no anomaly before the failure, the important independent variables for the vertical force are the conventional ones, namely a constant, the angle of attack α and pitch rate $\frac{q\bar{c}}{V}$. However, after the failure a violent roll-dive manoeuvre follows. The influence of the damage on the change in aerodynamics is represented by additional contributions by sideslip β and roll rate $\frac{pb}{2V}$. These are a consequence of the asymmetric damage, as a result of which

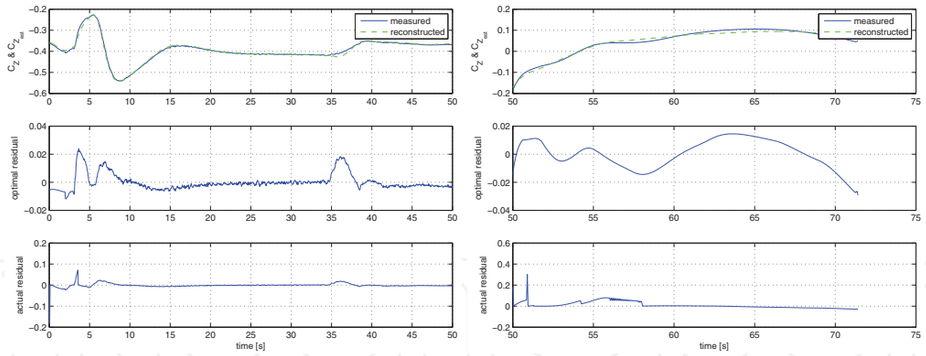

(a) AROLS structure selection and parameter estimation result for C_Z prior to failure

(b) AROLS structure selection and parameter estimation result for C_Z after failure

Fig. 5. AROLS structure selection and parameter estimation results for C_Z before and after the failure

the decoupling of longitudinal and lateral regressors does not hold anymore in this scenario. The standard deviations give an indication of the accuracy of the results.

	prior failure		post failure	
	estimated	(σ)	estimated	(σ)
1	-0.1583	(1%)	-0.4131	(2%)
α	-4.4016	$(\approx 0\%)$	4.9047	(1%)
$\frac{q\bar{c}}{V}$	-1.6124	(22%)	105.1966	(1%)
β	–	–	4.2319	(1%)
$\frac{pb}{2V}$	–	–	9.4708	$(\approx 0\%)$
$\frac{rb}{2V}$	–	–	–	–
all others	–	–	–	–

Table 4. SSPE results for C_Z for engine separation scenario, before and after failure

A more elaborate discussion of this example can be found in ref. Lombaerts et al. (2010c).

5. Fault Tolerant Control method

Fault Tolerant Flight Control is achieved by making use of a triple layered adaptive nonlinear dynamic inversion algorithm. First, the basics of the control approach are explained. Thereafter, each of the three individual control loops is described. Finally, some application examples on a selection of failure scenarios will show the failure handing capabilities of this fault tolerant control setup.

5.1 Control approach: Adaptive nonlinear dynamic inversion

A major advantage of dynamic inversion is its ability to naturally handle changes of operating condition, which removes the need for gain scheduling, e.g. as is the case for classical control methods. This is especially advantageous for control of space re-entry vehicles, due to their extreme and wide operating conditions which include hypersonic speed during re-entry and subsonic regions during the terminal glide approach phase to the runway. Another advantage is its natural property of decoupling the control axes, i.e. no coupling effects remain between

steering channels and the different degrees of freedom. NDI control has been implemented in the Lockheed F-35 Lightning II, (Balas (2003); Walker & Allen (2002)).
Nonlinear dynamic inversion considers original nonlinear systems of the affine form:

$$\dot{\mathbf{x}} = \mathbf{a}(\mathbf{x}) + \mathbf{b}(\mathbf{x})\,\mathbf{u} \tag{1}$$

and provides a solution for the physical control input $\mathbf{u}$ by introducing an outerloop virtual control input $\boldsymbol{\nu}$:

$$\mathbf{u} = \mathbf{b}^{-1}(\mathbf{x})\,[\boldsymbol{\nu} - \mathbf{a}(\mathbf{x})] \tag{2}$$

which results in a closed-loop system with a decoupled linear input-output relation:

$$\dot{\mathbf{x}} = \boldsymbol{\nu} \tag{3}$$

A linear outer loop control law is sufficient to enforce exponentially stable tracking dynamics, where the control gains can be determined by the required closed loop characteristics.
Dynamic inversion is a popular control method for flight control and aircraft guidance, (Balas et al. (1992); Campa et al. (2005); da Costa et al. (2003); Ramakrishna et al. (2001); Reiner et al. (1996); van Soest et al. (2006)) as well as reconfiguring control, (Ganguli et al. (2005; 2006); Oppenheimer & Doman (2006); Ostroff & Bacon (2002)).
The main assumption in NDI is that the plant dynamics are assumed to be perfectly known and therefore can be cancelled exactly. However, in practice this assumption is not realistic, not only with respect to system uncertainties but especially to unanticipated failures for the purpose of fault tolerant flight control. In order to deal with this issue, one can make use of robust control methods as outer loop control to minimize or suppress undesired behaviour due to plant uncertainties which cause imperfect plant dynamic cancellation. Other control methods such as neural networks also have been proposed in the literature, in order to augment the control signal as a compensation for the non-inverted dynamics, as explained previously. However, another solution to the weakness of classical NDI, namely its sensitivity to modelling errors, is the use of a real time identification algorithm, which supplies updated model information to the dynamic inversion controller. These augmented structures are called adaptive nonlinear dynamic inversion (ANDI). The latter procedure is the method of choice for this research which led to the results presented in this paper.

5.2 Autopilot control loops

Three consecutive inversion loops have been implemented, namely a body angular rate loop, an aerodynamic angle loop and a navigation loop. The developed control laws are described below.

5.2.1 Body angular rate loop

Consider the dynamic equation of an aircraft:

$$\dot{\boldsymbol{\omega}} = \mathbf{I}^{-1}\mathbf{M}_a - \mathbf{I}^{-1}\boldsymbol{\omega} \times \mathbf{I}\boldsymbol{\omega} \tag{4}$$

where $\boldsymbol{\omega} = \begin{bmatrix} p & q & r \end{bmatrix}^T$ are the rotational rates and $\mathbf{M}_a = \begin{bmatrix} L_a & M_a & N_a \end{bmatrix}^T$ the aerodynamic moments acting on the aircraft. The inertia matrix $\mathbf{I}$ stands for:

$$\mathbf{I} = \begin{bmatrix} I_{xx} & -I_{xy} & -I_{xz} \\ -I_{yx} & I_{yy} & -I_{yz} \\ -I_{zx} & -I_{zy} & I_{zz} \end{bmatrix} \tag{5}$$

where the moments of inertia I_{xy}, I_{yx}, I_{yz} and I_{zy} are assumed to be zero.

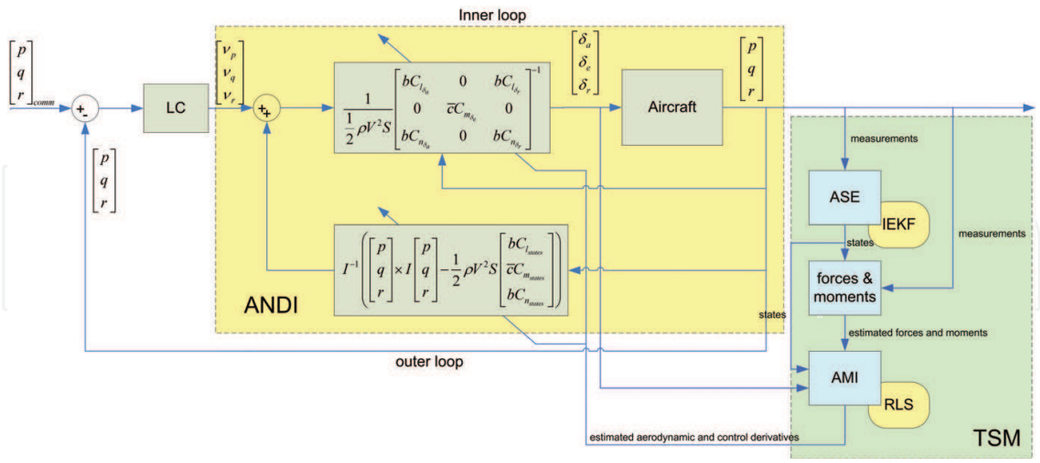

Fig. 6. NDI rate control inner loop

Rewriting the aircraft dynamics into the form of eq. (2):

$$\begin{bmatrix}\delta_a\\ \delta_e\\ \delta_r\end{bmatrix} = \begin{bmatrix} b\tilde{C}_{l_{\delta_a}} & 0 & b\tilde{C}_{l_{\delta_r}} \\ 0 & \bar{c}\tilde{C}_{m_{\delta_e}} & 0 \\ b\tilde{C}_{n_{\delta_a}} & 0 & b\tilde{C}_{n_{\delta_r}} \end{bmatrix}^{-1} \cdot \left\{ \left(\frac{1}{2}\rho V^2 S\right)^{-1} \left(\mathbf{I} \begin{bmatrix}\nu_p\\ \nu_q\\ \nu_r\end{bmatrix} + \begin{bmatrix}p\\ q\\ r\end{bmatrix} \times \mathbf{I} \begin{bmatrix}p\\ q\\ r\end{bmatrix} \right) - \begin{bmatrix} bC_{l_{\text{states}}} \\ \bar{c}C_{m_{\text{states}}} \\ bC_{n_{\text{states}}} \end{bmatrix} \right\} \tag{6}$$

where the virtual inputs $\begin{bmatrix}\nu_p & \nu_q & \nu_r\end{bmatrix}^T$ are the time derivatives of the rotational rates of the aircraft. All control and state derivatives in this expression are estimated via the real time identification procedure.

5.2.2 Aerodynamic angle loop

The middle loop quantities are roll angle ϕ, angle of attack α and sideslip angle β:

$$\begin{bmatrix}p\\ q\\ r\end{bmatrix} = \begin{bmatrix} -\frac{1}{\frac{v_b}{\sqrt{V^2-w_b^2}}} & \frac{\sin\phi\tan\theta}{\frac{u_b}{\sqrt{V^2-w_b^2}}} & \frac{\cos\phi\tan\theta}{0} \\ \frac{w_b}{\sqrt{V^2-v_b^2}} & 0 & \frac{-u_b}{\sqrt{V^2-v_b^2}} \end{bmatrix}^{-1} \cdot \left\{ \begin{bmatrix}\nu_\phi\\ \nu_\alpha\\ \nu_\beta\end{bmatrix} - \begin{bmatrix} 0 \\ -\frac{1}{\sqrt{V^2-w_b^2}}\left(A_z + g\cos\theta\cos\phi\right) \\ \frac{1}{\sqrt{V^2-v_b^2}}\left(A_y + g\cos\theta\sin\phi\right) \end{bmatrix} \right\} \tag{7}$$

5.2.3 Navigation loop

The procedure used in this step is inspired by the method used in ref. Holzapfel (2004), although the application for this study implies some important deviations compared to the conventional method, since an adaptive model needs to be taken into account. Main crux in this deviating approach is that this inversion loop consists of two separate steps. First, the

kinematics based virtual inputs are transformed towards the roll angle and the symmetric aerodynamic forces through a physically interpretable nonlinear mapping. Consequently, the aforementioned force components are translated into commanded angle of attack and dimensionless thrust values via a classical NDI-setup as used before, which involves a local gradient determination step.
The kinematics based inversion is as follows:

$$F_{A_X} = m\left(\dot{V} + g\sin\gamma\right) \tag{8}$$

$$F_{A_Z} = -\cos\gamma\sqrt{m^2\left[\left(g + \frac{V\dot{\gamma}}{\cos\gamma}\right)^2 + (V\dot{\chi})^2\right] - \left(\frac{F_{A_Y}}{\cos\gamma}\right)^2} \tag{9}$$

$$\mu = \arctan\left(\frac{\dot{\chi}\cos\gamma}{\dot{\gamma} + g\frac{\cos\gamma}{V}}\right) \tag{10}$$

where F_{A_Z} corresponds to $|F_{\text{required}}|$ and μ is in fact μ_{required}.
The subsequent aerodynamic forces based inversion is as follows:

$$\begin{pmatrix} \alpha \\ T_C \end{pmatrix} = \begin{pmatrix} F_{A_{X_\alpha}} & F_{A_{X_{T_C}}} \\ F_{A_{Y_\alpha}} & F_{A_{Y_{T_C}}} \\ F_{A_{Z_\alpha}} & F_{A_{Z_{T_C}}} \end{pmatrix}^{\dagger} \left[\begin{pmatrix} F_{A_{X\text{comm}}} \\ F_{A_Y} \\ F_{A_{Z\text{comm}}} \end{pmatrix} - \begin{pmatrix} F_{A_{X_0}} \\ F_{A_{Y_0}} \\ F_{A_{Z_0}} \end{pmatrix} \right] \tag{11}$$

where the symbol † denotes the left inverse.
More information about how these control laws have been derived in detail can be found in ref. Lombaerts (2010); Lombaerts et al. (2010b). Summarizing, the global setup of the third dynamic inversion loop can be found in figure 7.

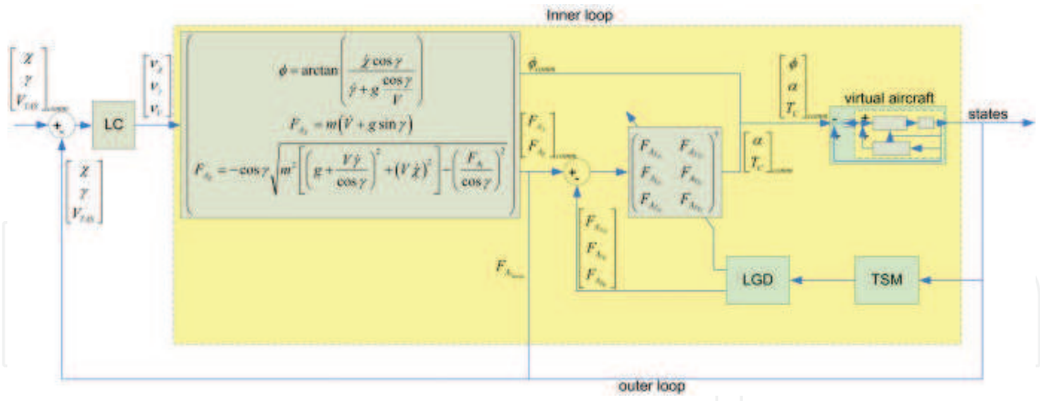

Fig. 7. Third NDI autopilot loop, featuring V_{TAS}, γ and χ control. LGD stands for local gradient determination. TSM represents the two step method model identification block elaborated in section 4.

Linear controllers act on each separate NDI loop, as indicated by "LC" in fig. 6 and 7. These linear controllers involve proportional and proportional-integral control, and gains have been selected to ensure favourable flying qualities by means of damping ratio ζ and natural frequency ω_n while complying with the time scale separation principle. Optimization of these gain values has been achieved by means of multi-objective parameter synthesis (MOPS) optimization, see ref. Lombaerts (2010); Looye (2007); Looye & Joos (2006).

5.3 Evaluations of autopilot experiments on RECOVER

Implementation of these control laws results in the controller performance illustrated in the following simulation results. Besides the unfailed scenario the following failures have been investigated: vertical tail loss and engine separation. In each scenario, the failure occurs exactly at $t = 50s$.

5.3.1 Nominal unfailed

A complex manoeuvre is performed to evaluate the performance of the fault tolerant controller. Three joint commands are given, more precisely a course change of $\Delta\chi = 160°$ at $t = 70s$, an altitude change towards $h = 5000m$ at $t = 80s$ and a velocity change of $\Delta V = 50m/s$ around $t = 110s$. This scenario allows to evaluate the performance as well as eventual inadvertent couplings between the different channels. The tracking of the reference signals is satisfactory and couplings are minimal to even non-existent, as can be seen in fig. 8. In the control surface deflection time histories in figures 9 and 10(a), it can be seen that the elevators compensate first for the vertical lift component loss induced by the turn, and then initiate the altitude change. Ailerons and rudders cooperate in order to achieve a coordinated turn. It can be seen that the spoilers assist the ailerons to set the turn up. The specific forces in fig. 10(b) indicate an acceptable behaviour. The responses of the unfailed aircraft will serve as a comparison basis to evaluate the performance of the controller in failed situations.

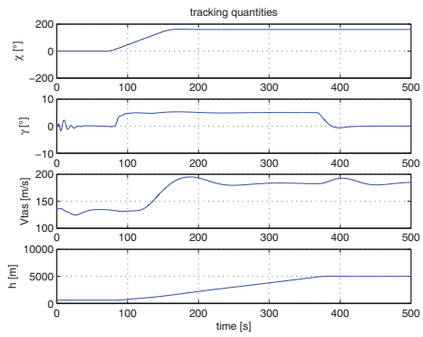

(a) tracking quantities

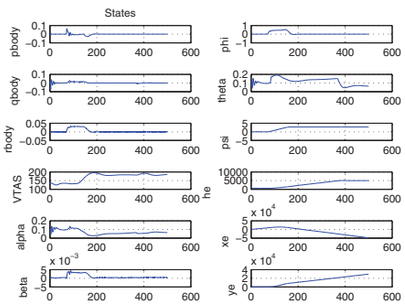

(b) states

Fig. 8. Tracking quantities and states for the unfailed scenario

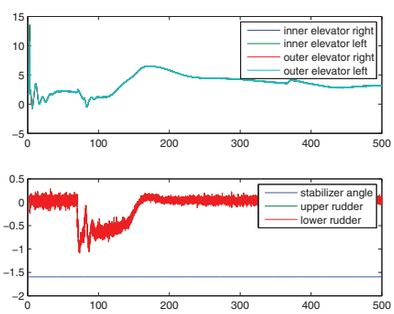

(a) deflections of elevators, stabilizer and rudders

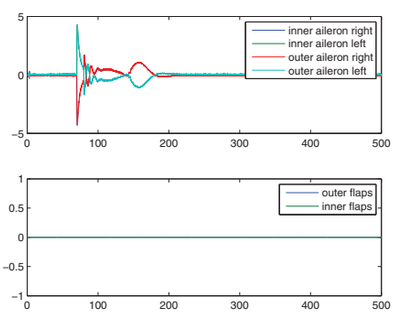

(b) deflections of ailerons and flaps

Fig. 9. Deflections of elevators, stabilizer, rudders, ailerons and flaps for the unfailed scenario

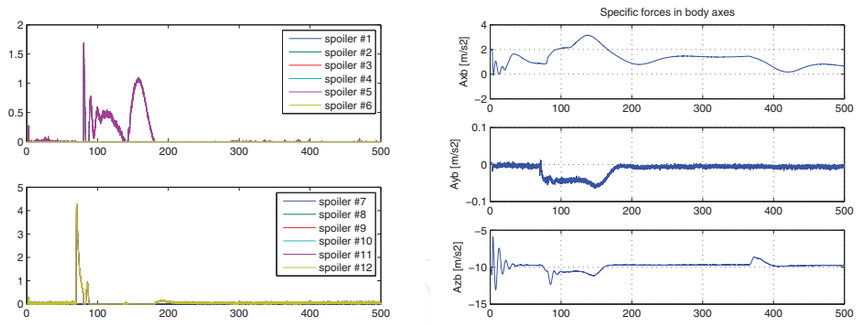

(a) deflections of spoilers (b) specific forces

Fig. 10. Deflections of spoilers and specific forces for the unfailed scenario

5.3.2 Vertical tail loss

For this failure scenario, the reference signals have been slightly adapted. No speed change is requested here, because this makes it more demanding for the control surfaces. When the speed increase is maintained, the increasing aerodynamic damping reduces the disturbing effect of the failure. The altitude capture has been changed accordingly to $1500m$, in order to prevent throttle saturation. Aerodynamic damping is the very reason why, in practice, control laws actually work with calibrated airspeed CAS, in this way the control actions are related to the dynamic pressure and control surface efficiency is maintained.

Figure 12(b) reveals the compensating behaviour of the ailerons which takes into account the loss of the vertical tail and the cessation of rudder functioning after failure, as can be seen in fig. 12(a). It can be observed that the ailerons effectively take over the function of yaw damper, assisted by the spoilers in fig. 13(a), since the rudders are lost. Figure 13(b) shows that the oscillation in the lateral specific force A_y is only damped in the longer term, which can be explained by the fact that ailerons and spoilers have no direct influence on the yawing moment, but on the rolling moment.

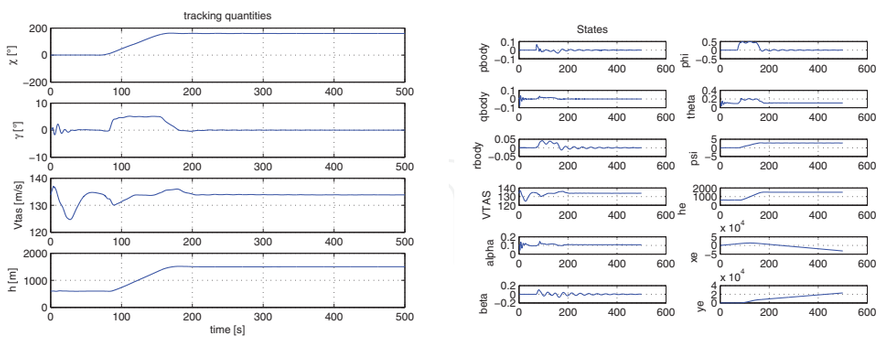

(a) tracking quantities (b) states

Fig. 11. Tracking quantities and states for the tail loss scenario

5.3.3 Engine separation

The engine separation scenario is a very sensitive situation to combine commands in heading, altitude and speed simultaneously. Crucial in this context is to avoid engine throttle saturation. Therefore, in this experiment only a heading change has been considered, as shown

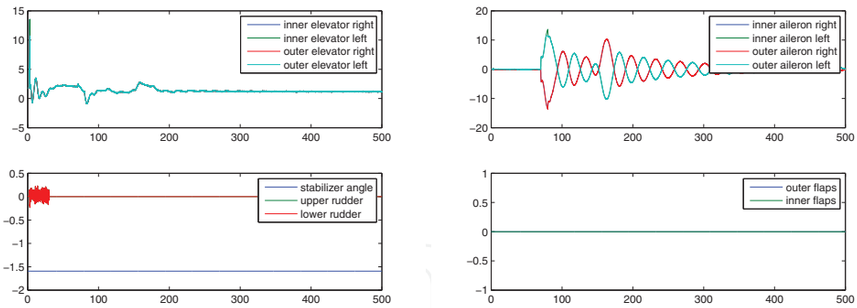

(a) deflections of elevators, stabilizer and rudders

(b) deflections of ailerons and flaps

Fig. 12. Deflections of elevators, stabilizer, rudders, ailerons and flaps for the tail loss scenario

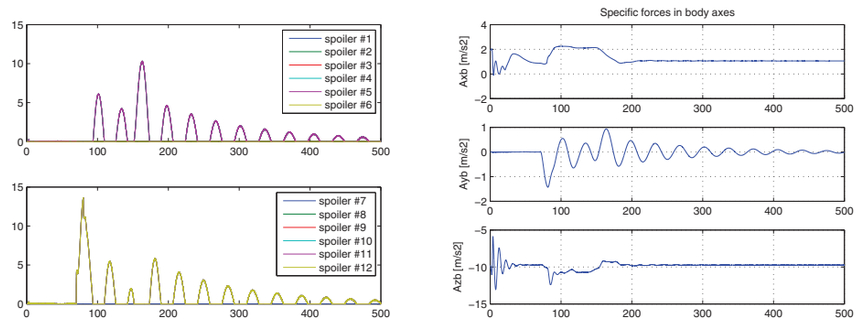

(a) deflections of spoilers

(b) specific forces

Fig. 13. Deflections of spoilers and specific forces for the tail loss scenario

in fig. 14(a). Moreover, a limited maximum roll angle has been imposed, due to the restricted safe flight envelope as explained in section 3. It has been found that altitude and speed changes are also feasible separately, but these are not discussed in this section.

The time histories of the states in fig. 14(b) reveal that the aircraft in post failure conditions flies with a small nonzero roll angle and sideslip angle, due to the asymmetric damage, despite a zero commanded sideslip angle. The control surface deflections in figures 15 and 16(a) confirm the cessation of functioning of the control surfaces which are powered by the hydraulic circuits connected to engines number 3 and 4, as illustrated in fig. 2(b). The remaining operative surfaces are successful in keeping the aircraft in equilibrium and under control, although with restricted authority. The nonzero lateral specific force in fig. 16(b) is a consequence of the sideslipping flight.

Two additional interesting quantities to investigate are the throttle setting and the average square innovation, which triggers the re-identification routine as explained in ref. Lombaerts et al. (2009; 2010a). Figure 17(a) confirms that the throttle setting does not saturate, however the remaining control margins in order to remain inside the safe flight envelope are severely restricted. This is due to the asymmetric thrust which needs to be compensated by the control surfaces. The spike at $t = 50s$ is caused by the feedforward path in the controller, which is needed to compensate for the instantaneous speed loss of the two dead engines. Figure 17(b) depicts the values for the average square innovation for each force and moment channel separately. At $t = 50s$, it can be seen that the threshold for $\overline{\Delta}_X$ is exceeded, and a

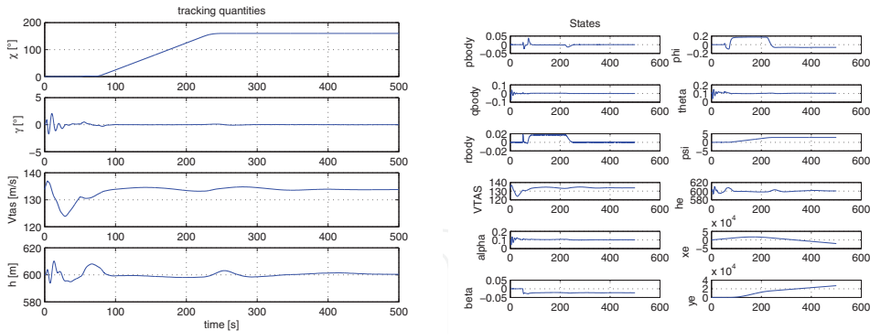

(a) tracking quantities (b) states

Fig. 14. Tracking quantities and states for the engine separation scenario

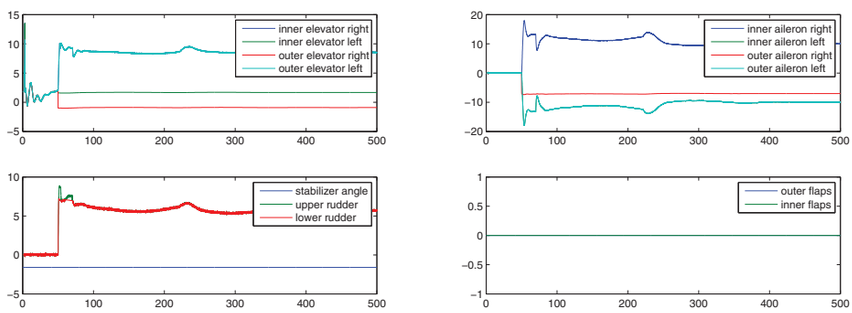

(a) deflections of elevators, stabilizer and rudders (b) deflections of ailerons and flaps

Fig. 15. Deflections of elevators, stabilizer, rudders, ailerons and flaps for the engine separation scenario

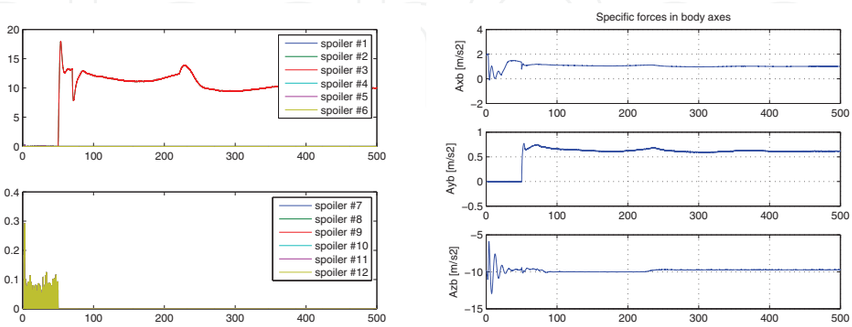

(a) deflections of spoilers (b) specific forces

Fig. 16. Deflections of spoilers and specific forces for the engine separation scenario

re-identification procedure is triggered for C_X. It has become necessary to include the sideslip angle β, which has become significant due to the sideslipping flight, as an additional regressor in the identification procedure. This leads to a successful new identification procedure which is performed extremely quickly as can be seen in this figure. This result confirms the beneficial contribution from the identification routine in this fault tolerant flight control setup.

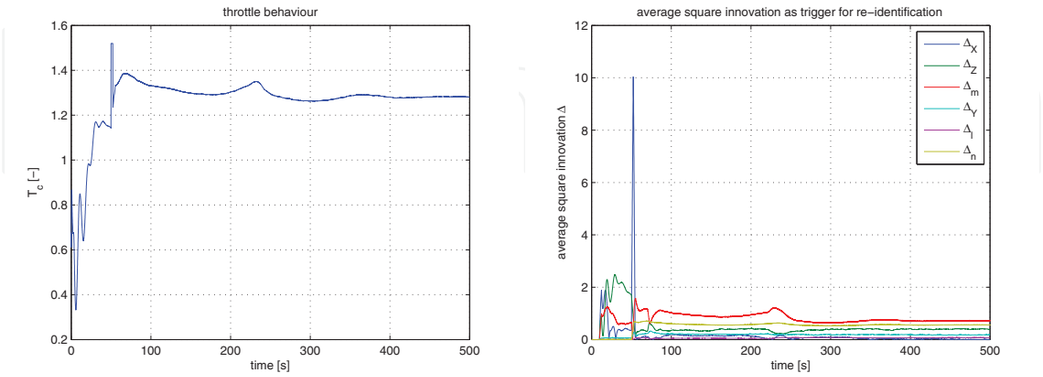

(a) throttle behaviour

(b) average square innovation as trigger for re-identification

Fig. 17. Spoilers and specific forces for the engine separation scenario

5.4 Manual control loops

A manual variant of this fault tolerant controller has been developed as well. This variant consists of the body angular rate inner loop as described in section 5.2.1, augmented by the sideslip β coordination axis only from the aerodynamic angle middle loop as explained in section 5.2.2. Throttle control is by the conventional autothrottle. As a result, the pilot steers roll rate p by means of the control wheel, pitch rate q with the control columns, and finally the pedals can be used for creating a nonzero sideslipping flight, although this is rarely used. Since dynamic inversion is used in all control loops, these steering channels are effectively decoupled.

5.5 Simulator evaluation of manual controller

This manual control setup has been applied in the SIMONA (SImulation, MOtion and NAvigation) Research Simulator (SRS), see fig.18(a). It is a pilot-in-the-loop flight simulator developed, built and operated by Delft University of Technology. It provides researchers with a flexible powerful tool that can be adapted to various uses, see ref. Stroosma et al. (2003). The simulator's flexible software architecture and high-fidelity cueing environment allows the integration of a variety of aircraft simulation models, such as the aforementioned Boeing 747 benchmark simulation model from ref. Smaili et al. (2006). Its inputs and outputs were standardized to fit the SRS software environment and the SIMULINK^{TM} simulation model as well as NDI-controller were converted to C code using Real-Time Workshop. Finally the models were integrated with the pilot controls, aircraft instruments (Figure 18(b)) and other cueing devices of the SRS (i.e. outside visual and motion systems). On the flight deck of the SRS the evaluation pilot was presented with flight instruments representative of a large transport aircraft, a control column with large transport aircraft feel system dynamics, a central pedestal with dual engine controls and a wide collimated view on a virtual outside world. The simulator's motion system was tuned to give the pilot realistic inertial motion

cues in nominal and failure conditions. The test pilots were four Boeing 747 captains (one retired) and one other wide body captain on Airbus A330 and Boeing 767. All were familiar with the research simulator practices used for this investigation.

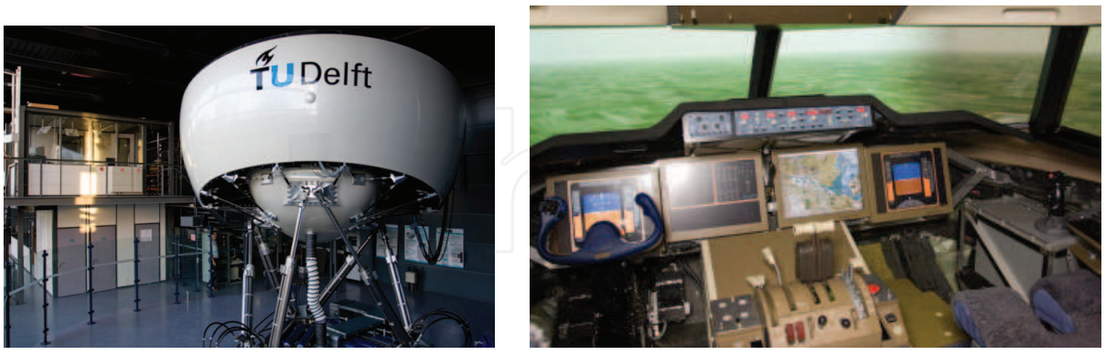

(a) outside view (b) cockpit view

Fig. 18. The SIMONA (SImulation, MOtion and NAvigation) Research Simulator (SRS) at Delft University of Technology, photo by Joost Ellerbroek

The adaptive NDI control system has been validated on two failure scenarios, namely the engine separation failure and the rudder runaway scenarios. Fig. 19 shows the evaluation trajectory during the piloted simulation runs in SIMONA. The trajectory consists of four main phases, namely altitude capture, bank angle capture, localizer intercept and glideslope intercept. For every phase, required and adequate performance specifications have been defined for the relevant longitudinal as well as lateral quantities. The scheme presented in fig. 20 assists the pilot in rating the handling qualities (Cooper & Harper (1969)) of the aircraft while taking into account the performance of the aircraft with respect to the aforementioned requirements. Fig. 21 shows the time histories of a selection of the most important aircraft states. These confirm the evaluation trajectory as shown in fig. 19. Moreover, altitude and roll angle plots show altitude and roll angle captures which have been executed by the test pilot in order to evaluate the post-failure handling qualities of the aircraft.

The handling qualities results for the algorithm show that, especially for the El Al Flight 1862 scenario, conventional flight control was restored to acceptable levels while physical and mental workload were reduced significantly. This is illustrated in Figure 22 where an example is given of lateral handling quality pilot ratings for the localizer capture task. It can be seen that, for this task, both the baseline and fault-tolerant fly-by-wire (FBW) aircraft were rated Level 1 (Rating 1-3). After separation of the right-wing engines (Figure 22), lateral handling qualities degraded to Level 2 for the conventional aircraft with the classical control system. The reconfigured aircraft (FBW) shows about Level 1 handling qualities after incurring significant damage due to the loss of the right-wing engines. This was substantiated by measured pilot control activities, representative of workload, indicating no pilot compensation after reconfiguration. For the rudder runaway failure, however, Level 2 handling qualities remained after reconfiguration despite the fact that no sustained pilot compensation was required. The difference was most probably caused by the fact that this initial setup is a rate control and hold loop instead of a rate control attitude hold type. As a consequence, angular rate disturbances are corrected for automatically by the controller but subsequent disturbances from the equilibrium attitude had to be compensated for by the pilot himself. The use of a rate control attitude hold setup will solve this issue.

Figure 23 illustrates the physical workload analysis results by depicting the average pilot forces. In the graph, a distinction is made between roll, pitch and yaw channel, as illustrated

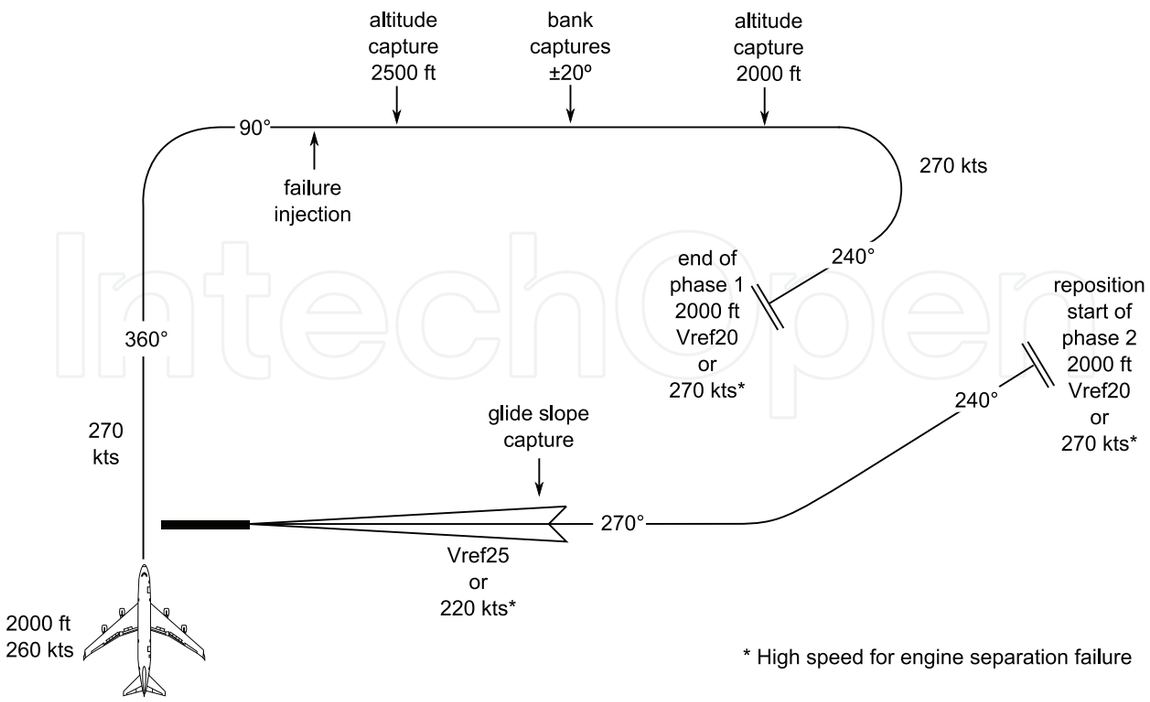

Fig. 19. Trajectory of the piloted simulation runs in SIMONA.

by the three graphs separated vertically. In each control channel, six cases have been studied, namely unfailed, engine separation and rudder runaway, each time with classical and fault tolerant control. In each case, the workload figure of each of the five pilots is represented individually by means of bar plots, after which the mean and standard deviations are superimposed on these bar plots for every case, in order to facilitate mutual comparisons.

First of all, the unfailed conditions confirm that this is a good comparison basis between classic and FTFC, since both have the same ratings. Comparing classic control with FTFC for failed configurations shows that overall values for average manual control forces over all pilots decrease for FTFC in the failure scenarios. In addition, in the failure scenarios the standard deviations also reduce from classic control towards FTFC. At first sight this seems not the case for the pedal forces. Closer inspection of the experimental data, however, reveals that this is caused by the deviating performance of pilot no 2 (probably due to misconception of the control principle within the fault tolerant controller). Finally, searching for overlap of the errorbars between classic and FTFC shows that this overlap does not occur. This observation makes the trends significant, despite the limited number of experiment subjects.
As a global conclusion, which is supported by the graphs above, it can be stated that this fault tolerant flight controller improves the handling qualties and reduces physical pilot workload considerably in failure conditions.

6. Conclusions and future work

Summarizing, it can be stated that, following numerous experiments, fault tolerant flight control using a physical modular approach is successful in recovering damaged aircraft. The designed methods are capable to accommodate the damage scenarios which have been investigated in this project. It has been found that the engine separation scenario, based upon

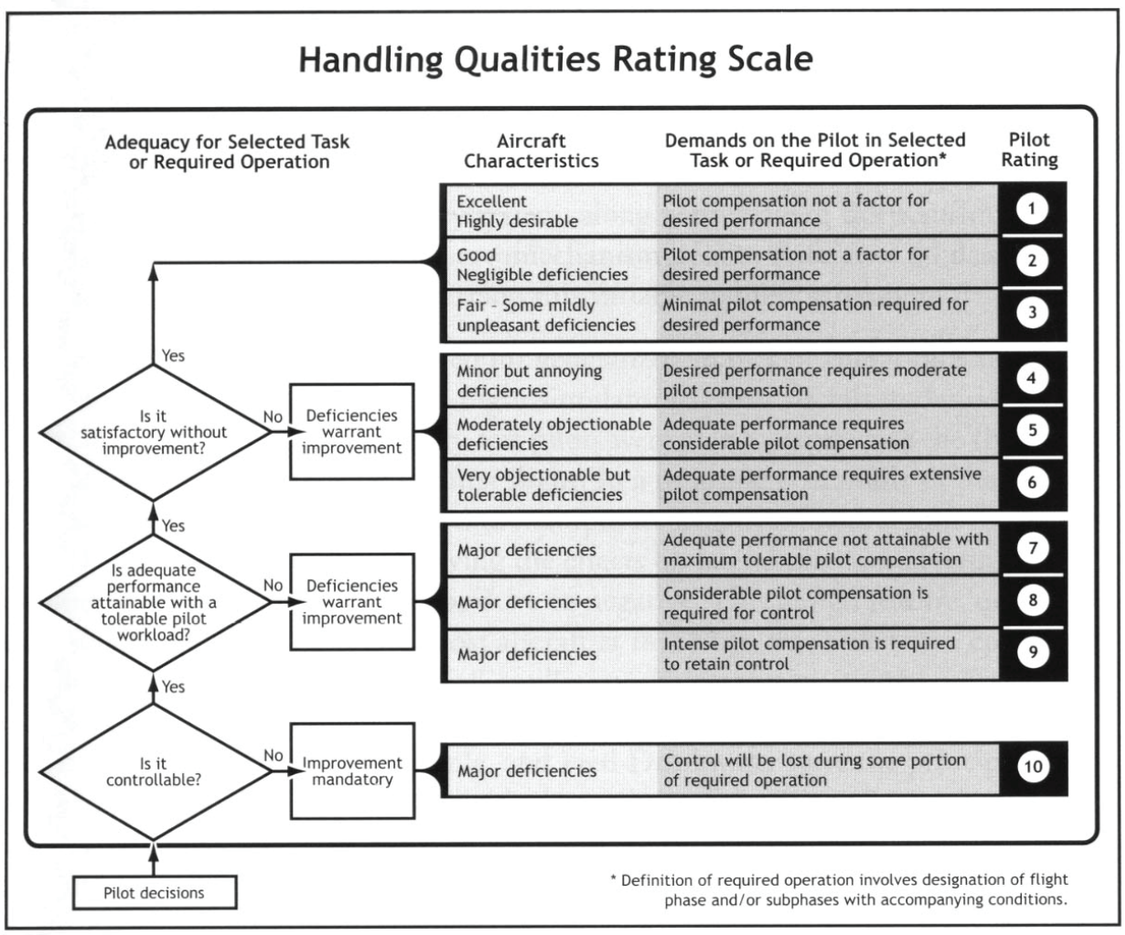

Fig. 20. Cooper Harper Handling Qualities Rating Scale, source: Cooper & Harper (1969)

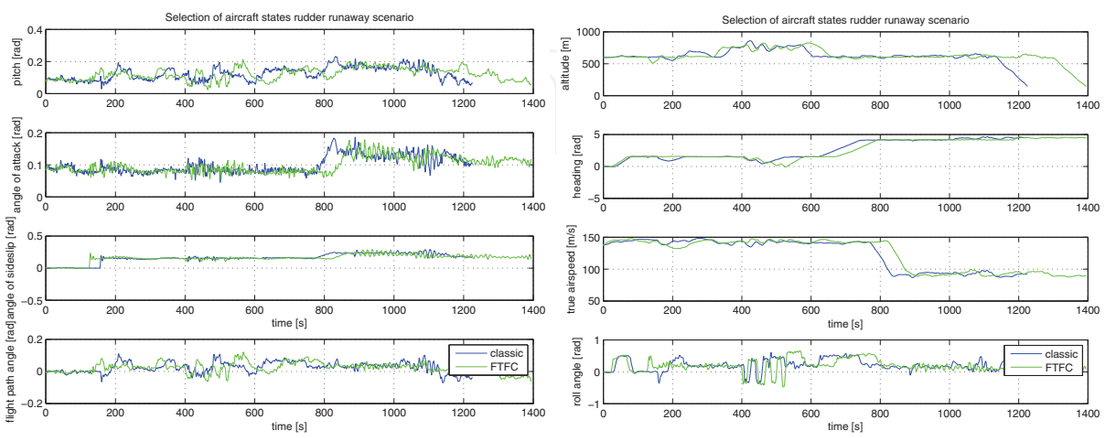

Fig. 21. Comparison of a selection of aircraft states for the rudder runaway scenario

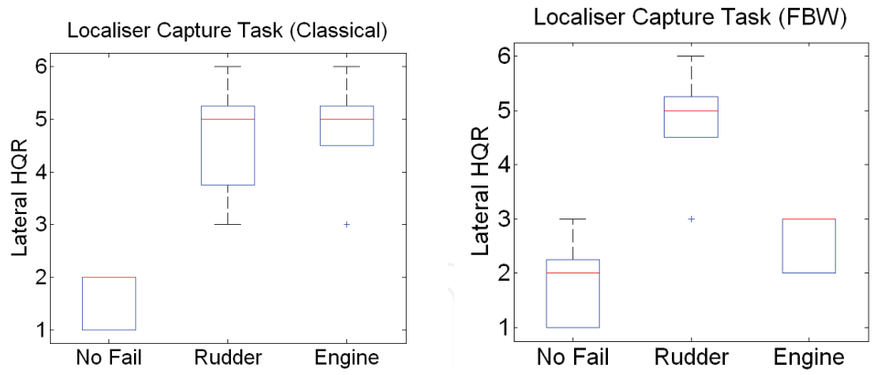

(a) classical control (b) fault tolerant control

Fig. 22. Localizer capture task handling qualities ratings for classical control and fault tolerant control

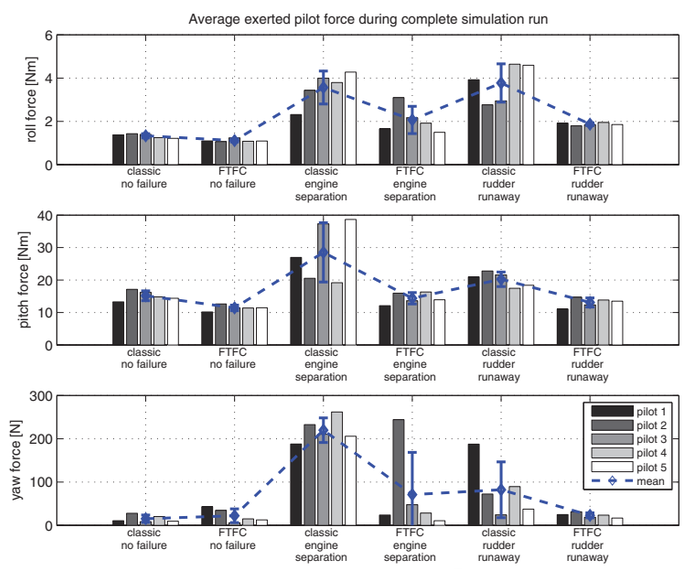

Fig. 23. Total average manual control forces during the simulation runs

El Al flight 1862, is survivable with adaptive control techniques. Experiments have also shown that the two step method is successful for real time identification of damaged aircraft models, including a real time static stability analysis. Autopilot control based upon adaptive nonlinear dynamic inversion shows good failure handling capabilities.
An important aspect which has not been considered in this research is sensor loss detection. Despite the presence of redundant sensors, recent aircraft accidents (Lombaerts (2010)) have shown that sensor loss detection cannot be avoided and current monitoring techniques are not always sufficient. More elaborate flight envelope protection algorithms, taking into account a.o. minimum control airspeed limits, are another important topic for future research. Finally, an important next step in the development of fault tolerant flight control technologies is to validate them in real flight on board of manned as well as unmanned research aircraft. This is one of the major challenges for the future.

7. References

Alwi, H. (2008). *Fault Tolerant Sliding Mode Control Schemes with Aerospace Applications*, PhD thesis, University of Leicester.

Balas, G. (2003). Flight control law design: An industry perspective, *European Journal of Control, special issue* 9(2–3): 207–226.

Balas, G., Garrard, W. & Reiner, J. (1992). Robust dynamic inversion control laws for aircraft control, *Proceedings of the AIAA Guidance, Navigation and Control Conference*, AIAA, Washington, DC, pp. 192–205.

Brinker, J. & Wise, K. (1999). Nonlinear simulation analysis of a tailless advanced fighter aircraft reconfigurable flight control law, *AIAA Guidance, Navigation and Control Conference and Exhibit*, number AIAA-99-4040, Portland, OR.

Calise, A. J., Lee, S. & Sharma, M. (2001). Development of a reconfigurable flight control law for the x-36 tailless fighter aircraft, *AIAA Journal of Guidance, Control and Dynamics* 24(5): 896–902.

Campa, G., Seanor, B., Gu, Y. & Napolitano, M. R. (2005). Nldi guidance control laws for close formation flight, *American Control Conference*, Portland, OR, USA.

Chu, Q. (2007). *Lecture Notes AE4-394, Modern Flight Test Technologies and System Identi□cation*, Delft University of Technology, Faculty of Aerospace Engineering.

Chu, Q., Mulder, J. & Sridhar, J. (1994). Decomposition of aircraft state and parameter estimation problems, *Proceedings of fhe 10th IFAC Sympium on System Identi□ation*, Vol. Vol. 3, pp. pp. 61–66.

Cieslak, J., Henry, D., Zolghadri, A. & Goupil, P. (2008). Development of an active fault-tolerant flight control strategy, *AIAA Journal of Guidance, Control and Dynamics* 31: 135–147.

Civil Aviation Safety Data 1993-2007 (2008). *Technical report*, Civil Aviation Authority of the Netherlands (CAA-NL).

Cooper, G. & Harper, R. J. (1969). The use of pilot rating in the evaluation of aircraft handling qualities, *Technical Report TN D-5153*, NASA.

Corvin, J. H., Havern, W. J., Hoy, S. E., Norat, K. F., Urnes, J. M. & Wells, E. A. (1991). Self-repairing flight control systems, volume i: Flight test evaluation on an f-15 aircraft, *Final Report WL-TR-91-3025*.

da Costa, R., Chu, Q. P. & Mulder, J. A. (2003). Re-entry flight controller design using nonlinear dynamic inversion, *Journal of Spacecraft and Rockets* 40(1): 64–71.

Ganguli, S., Papageorgiou, G., Glavaski, S. & M., E. (2005). Piloted simulation of fault detection, isolation and reconfiguration algorithms for a civil transport aircraft, *AIAA Guidance, Navigation and Control Conference and Exhibit*, number AIAA-2005-5936, San Francisco, CA.

Ganguli, S., Papageorgiou, G., Glavaski, S. & M., E. (2006). Aircraft fault detection, isolation and reconfiguration in the presence of measurement errors, *AIAA Guidance, Navigation and Control Conference and Exhibit*, number AIAA-2006-6551, Keystone, Co.

Gavrilets, V. (2008). Damage tolerant flight control systems for unmanned aircraft, *ICAS/ATIO Conference*.

Hallouzi, R. & Verhaegen, M. (2008). Fault-tolerant subspace predictive control applied to a boeing 747 model, *AIAA Journal of Guidance, Control and Dynamics* 31: 873–883.

Holzapfel, F. (2004). *Nichtlineare adaptive Regelung eines unbemannten Fluggerätes*, PhD thesis, Lehrstuhl für Flugmechanik und Flugregelung, Technische Universität München.

Intelligent Flight Control: Advanced Concept Program (1999). *Final Report BOEING-STL 99P0040*, The Boeing Company.

Jategaonkar, R. (2006). *Flight Vehicle System Identi□cation: A Time Domain Methodology*, Vol. 216 of *Progress in Astronautics and Aeronautics Series*, first edn, AIAA.

Joosten, D., van den Boom, T. & Lombaerts, T. (2007). Effective control allocation in fault-tolerant flight control with mpc and feedback linearization, *Proceedings of the European Conference on Systems and control*, Kos, Greece, pp. 3552–3559.

Joosten, D., van den Boom, T. & Lombaerts, T. (2008). Fault-tolerant control using dynamic inversion and model-predictive control applied to an aerospace benchmark, *the Proceedings of the 17th IFAC world congress*, Vol. 17, pp. 12030–12035.

KrishnaKumar, K. & Gundy-Burlet, K. (n.d.). Intelligent control approaches for aircraft applications, *Technical report*, NeuroEngineering Laboratory, NASA Ames Research Center.

Laban, M. (1994). *Online aircraft aerodynamic model identi□cation*, PhD thesis, Delft University of Technology.

Lombaerts, T. (2010). *Fault Tolerant Flight Control. A Physical Model Approach*, PhD thesis, Delft University of Technology.

Lombaerts, T., Breeman, J., Joosten, D., van den Boom, T., Chu, Q., Mulder, J. & Verhaegen, M. (2005). Specifications modelling document for Garteur AG16 fault tolerant control, *Technical report*, Delft University of Technology.

Lombaerts, T., Chu, Q., Mulder, J. & Joosten, D. (2007). Real time damaged aircraft model identification for reconfiguring control, *Proceedings of the AIAA AFM Conference and Exhibit*, number AIAA-2007-6717, Hilton Head, SC.

Lombaerts, T., Chu, Q.-P., Mulder, J. A. & Joosten, D. (2009). Flight control reconfiguration based on a modular approach, *Proceedings of the 7th IFAC SAFEPROCESS Symposium on Fault Detection, Supervision and Safety of Technical Processes*, pp. 259–264.

Lombaerts, T., Chu, Q.-P., Mulder, J. A. & Joosten, D. (2010a). Flight control reconfiguration based on a modular approach, *Control Engineering Practice* . under review.

Lombaerts, T., Joosten, D., J.H.Breemand, Smaili, H., Chu, Q., van den Boom, T., Mulder, J. & Verhaegen, M. (2006). Assessment criteria as specifications for reconfiguring control, *proceedings of the AIAA Guidance, Navigation, and Control Conference and Exhibit*, number AIAA-2006-6331, Keystone, CO.

Lombaerts, T., Looye, G., Chu, Q. P. & Mulder, J. A. (2010b). Pseudo control hedging and its application for safe flight envelope protection, *AIAA Guidance, Navigation and Control Conference and Exhibit*.

Lombaerts, T., Van Oort, E., Chu, Q. P., Mulder, J. A. & Joosten, D. (2010c). Online aerodynamic model structure selection and parameter estimation for fault-tolerant control, *Journal of Guidance, Control and Dynamics* . to be published.

Looye, G. (2007). *An Integrated Approach to Aircraft Modelling and Flight Control Law Design*, PhD thesis, Delft University of Technology.

Looye, G. & Joos, H.-D. (2006). Design of autoland controller functions with multiobjective optimization, *AIAA Journal of Guidance, Control and Dynamics* 29(2): 475–484.

Maciejowski, J. & Jones, C. N. (2003). Mpc fault-tolerant flight control case study: Flight 1862, *Proceedings of the 5th IFAC Symposium on Fault Detection, Supervision and Safety of Technical Processes SAFEPROCESS*, Washington DC, USA, pp. 121–126.

Marcos, A. & Balas, G. (2003). A boeing 747Ű100/200 aircraft fault tolerant and diagnostic benchmark, *Technical Report AEMŰUoMŰ2003Ű1*, Department of Aerospace and Engineering Mechanics, University of Minnesota.

Morelli, E. (2000). Real-time parameter estimation in the frequency domain, *Journal of Guidance, Control and Dynamics* 23(5): 812–818.

Mulder, J. (1986). *Design and evaluation of dynamic □ight test manoeuvers*, PhD thesis, TU Delft, Faculty of Aerospace Engineering.

Mulder, J., Chu, Q., Sridhar, J., Breeman, J. & Laban, M. (1999). Non-linear aircraft flight path reconstruction review and new advances, *Progress in Aerospace Sciences* 35(7): 673–726.

Mulder, J., van Staveren, W., van der Vaart, J. & de Weerdt, E. (January 2006). *Lecture Notes AE3-302, Flight Dynamics*, Delft University of Technology, Faculty of Aerospace Engineering, Delft, The Netherlands.

Oppenheimer, M. & Doman, D. (2006). Efficient reconfiguration and recovery from damage for air vehicles, *Proceedings of the AIAA Guidance, Navigation and Control Conference and Exhibit*, number AIAA-2006-6552.

Ostroff, A. J. & Bacon, B. J. (2002). Enhanced ndi strategies for reconfigurable flight control, *Proceedings of the American Control Conference*, Anchorage, AK.

Ramakrishna, V., Hunt, L. & Meyer, G. (2001). Parameter variations, relative degree, and stable inversion, *Automatica* 37: 871–880.

Reiner, J., Balas, G. J. & Garrard, W. L. (1996). Flight control design using robust dynamic inversion and time-scale separation, *Automatica* 32(11): 1493–1504.

Smaili, H., Breeman, J. & Lombaerts, T. (2008). A simulation benchmark for aircraft survivability assessment, *Proceedings of the International Congress of Aeronautical Sciences*, number 2008-9.3.2.

Smaili, M., Breeman, J., Lombaerts, T. & Joosten, D. (2006). A simulation benchmark for integrated fault tolerant flight control evaluation, *Proceedings of the AIAA Modelling and Simulation Technologies Conference and Exhibit*, number AIAA-2006-6471.

Stroosma, O., van Paassen, M. & Mulder, M. (2003). Using the simona research simulator for human-machine interaction research, *AIAA Modeling and Simulation Technologies Conference*.

Szaszi, I., Ganguli, S., Marcos, A., Balas, G. J. & Bokor, J. (2002). Application of fdi to a nonlinear boeing 747 aircraft, *10th Mediterranean Conference on Control and Automation*, Lisbon, Portugal.

van Soest, W., Chu, Q. P. & Mulder, J. A. (2006). Combined feedback linearization and model predictive control for re-entry flight, *AIAA Journal of Guidance, Control and Dynamics* 29(2): 427–434.

Varga, A. (2007). Design of least order residual generators for fault detection and isolation with application to monitoring actuator/surface faults for a boeing 747-100/200 aircraft, *Technical report*, German Aerospace Center (DLR).

Varga, A. & Hecker, S. (2004). Methods for threshold selection for robust residual evaluation, *Technical report*, German Aerospace Center (DLR).

Walker, G. & Allen, D. (2002). X-35b stovl flight control law design and flying qualities, *Proceedings of the Biennial International Powered Lift Conference and Exhibit*, number AIAA-2002-6018.

Ward, D. & Barron, R. (1995). A self-designing receding horizon optimal flight controller, *Proceedings of the American Control Conference*, Seattle, Washington.

Advances in Flight Control Systems

Edited by Dr. Agneta Balint

ISBN 978-953-307-218-0
Hard cover, 296 pages
Publisher InTech
Published online 11, April, 2011
Published in print edition April, 2011

Nonlinear problems in flight control have stimulated cooperation among engineers and scientists from a range of disciplines. Developments in computer technology allowed for numerical solutions of nonlinear control problems, while industrial recognition and applications of nonlinear mathematical models in solving technological problems is increasing. The aim of the book Advances in Flight Control Systems is to bring together reputable researchers from different countries in order to provide a comprehensive coverage of advanced and modern topics in flight control not yet reflected by other books. This product comprises 14 contributions submitted by 38 authors from 11 different countries and areas. It covers most of the currents main streams of flight control researches, ranging from adaptive flight control mechanism, fault tolerant flight control, acceleration based flight control, helicopter flight control, comparison of flight control systems and fundamentals. According to these themes the contributions are grouped in six categories, corresponding to six parts of the book.

InTech Europe
University Campus STeP Ri
Slavka Krautzeka 83/A
51000 Rijeka, Croatia
Phone: +385 (51) 770 447
Fax: +385 (51) 686 166
www.intechopen.com

InTech China
Unit 405, Office Block, Hotel Equatorial Shanghai
No.65, Yan An Road (West), Shanghai, 200040, China
中国上海市延安西路65号上海国际贵都大饭店办公楼405单元
Phone: +86-21-62489820
Fax: +86-21-62489821

IntechOpen